Oxidation functional groups on graphene: Structural and electronic properties

Jia-An Yan and M. Y. Chou
School of Physics, Georgia Institute of Technology, Atlanta, Georgia 30332-0430, USA
(Received 28 March 2010; revised manuscript received 22 July 2010; published 2 September 2010)

We presented a detailed study of the oxidation functional groups (epoxide and hydroxyl) on graphene based on density-functional calculations. Effects of single functional groups and their various combinations on the electronic and structural properties are investigated. It is found that single functional groups can induce interesting electronic bound states in graphene. Detailed energetics analysis shows that epoxy and hydroxyl groups tend to aggregate on the graphene plane. Investigations of possible ordered structures with different compositions of epoxy and hydroxyl groups show that the hydroxyl groups could form chainlike structures stabilized by the hydrogen bonding between these groups, in close proximity of the epoxy groups. Our calculations indicate that the energy gap of graphene oxide can be tuned in a large range of 0–4.0 eV, suggesting that functionalization of graphene by oxidation will significantly alter the electronic properties of graphene.

DOI: 10.1103/PhysRevB.82.125403 PACS number(s): 73.61.Wp, 73.20.−r, 73.22.−f

I. INTRODUCTION

Oxidation of graphene has recently been under intense study owing to its fundamental interest and potential applications.[1–3] More importantly, oxidation of graphene serves as an example for chemical functionalization of graphene,[4–7] which is of great interest to tune the electronic, mechanical, and optoelectronic properties of graphene. Many interesting properties of graphene oxide have been reported.[5,8–10] Furthermore, chemical reduction in graphene oxide has been demonstrated as a promising solution-based route for mass production of graphene.[3,11–16]

Graphene oxide is a single layer of graphite oxide and can be fabricated using different chemical methods. Depending on the fabrication processes and conditions, graphene oxide can have very different compositions.[17] The lower and upper limits of the C:O:H ratio are 6:2.33:1.2 and 6:3.7:2.83, respectively.[18] This amorphous nature has imposed big challenges for understanding its atomic structure for more than a century. Ruess[19] first proposed that the carbon layers were puckered and that the oxygen-containing groups were hydroxyl and etherlike oxygen bridges between 1 and 3 carbon atoms, randomly distributed on the carbon skeleton. Based on the Ruess model, Hofmann and co-workers[20] suggested that part of the hydroxyl groups are adjacent to C═C double bonds. In 1991, Mermoux *et al.*[21] confirmed the existence of ether bridges, hydroxyl groups, and sp^2 coordinated carbons, based on their FTIR and ^{13}C NMR studies. These authors also proposed an ideal stoichiometrical structure of $C_8O_2(OH)_2$, corresponding to the local ordering of the three building blocks.

On the other hand, Nakajima *et al.*[17,22] proposed a different model for graphite oxide according to the fact that the fluorination of graphite oxide yields the same x-ray diffraction pattern as stage-2-type graphite fluoride $(C_2F)_n$. This structure model is an intermediate form between two ideal structures, $C_8(OH)_4$ and C_8O_2, consisting of double carbon layers linked with each other by sp^3 bonds perpendicular to the carbon network. The carbonyl and hydroxyl groups are combined with the double carbon layers from above and below. It has a structure with sixfold symmetry (hexagonal system $6m2$) with the stacking sequence A-A′/B-B′ of carbon layers. Oxygen forms double bond with carbon, and there is no epoxy group in this structure. This model, which involves two layer graphene sheets with sp^3 bond in between, is distinct from previous ones, which essentially have single graphene sheets.

Later, He and Lerf[23,24] further established that the main functional groups on graphene oxide are epoxy (1,2-ether, not 1,3-ether) and hydroxyl groups, with some hydroxyl, carbonyl, and carboxyl groups at the edge. Based on the experimental results, the authors suggested that graphene oxide might contain aromatic "islands" of variable size which have not been oxidized. These islands are separated from each other by aliphatic six-membered rings containing C—OH, epoxy groups, and double bonds. More recently, a high-resolution solid-state ^{13}C-NMR measurement[25] has confirmed the existence of C—OH (hydroxyl), C—O—C (epoxy), and sp^2 C units on these layers. The data further indicate that a large fraction of sp^2 C atoms are bonded directly to C atoms in the hydroxyl and epoxy groups, and that a large fraction of C atoms in the hydroxyl and epoxide units are bonded to each other.

On the theoretical side, Kudin *et al.*[26] studied the structures for functionalized graphene by calculating the Raman spectra and comparing them with experimental data. A graphene oxide model containing areas of sp^2 carbons with an alternating pattern of single-double carbon bonds is used to explain the experimentally observed blue shift of the G band in graphene oxide. Through computational Monte Carlo simulation, Paci *et al.*[27] found that the hydrogen bonding between epoxy and hydroxyl groups and between hydroxyl groups may have significant impact on the stability of many structures. Density-functional calculations are also performed by Boukhvalov and Katsnelson to study the structures of graphene oxide.[28] More recently, oxidation of graphene by only epoxy groups[29] and at various oxidation levels[30] are reported. An atomic mechanism to cut the graphene sheet via epoxy pair is also proposed.[31]

In spite of many models proposed in the literature, the exact structures of graphene oxide remain unresolved.[17,21–24]

Since the electronic properties of graphene oxide significantly depend on the exact structure, it is highly desirable to establish the microscopic atomic picture of graphene oxide. In our previous work,[32] we reported preliminary results from first-principles calculations that address the energetically favorable building blocks and stable phases in graphene oxide. The current paper provides a complete report on the possible structures of the functional groups and their effects on the electronic properties of graphene.

The paper is organized as follows: In Sec. III A, the effects of a single functional group on graphene are studied. We will discuss the structural distortions induced, and the change in the graphene band structure. Interesting localized electronic states are found. In Sec. III B, various combinations of the functional groups on graphene are investigated and their preference to aggregate on graphene will be discussed. Localized vibrational features are also reported for some low-energy configurations. In Sec. III C, based on these building blocks, we study some possible ordered phases. Finally, a summary is given in Sec. IV.

II. CALCULATIONAL DETAILS

Density-functional calculations are carried out using the local-density approximation (LDA) with a plane-wave basis as implemented in the Vienna *ab initio* simulation package (VASP).[33] Vanderbilt ultrasoft pseudopotentials[34] are employed. All calculations are performed with a plane-wave cutoff energy of 500 eV. For configurations with a single functional group, we have used graphene supercells with size varying from 2×2 to 6×6 in order to check the convergence as well as the change in the electronic properties of graphene. An equivalent Monkhorst-Pack[35] k grid of 24×24 for a 1×1 graphene unit cell is used in all calculations. For various combinations of functional groups, we found that a 5×5 supercell is large enough for the energetics analysis. The 5×5 unit cell contains 50 C atoms, providing a separation of 12.3 Å for the atomic combinations under investigation. The vertical size of the supercell is 12 Å so the interaction between the layers is expected to be minimal. The size and shape of the two-dimensional unit cell are optimized for different coverages. The optimization of atomic positions proceeds until the change in energy is less than 1×10^{-6} eV per cell and the force on each atom is less than 0.02 eV/Å. In slab-type supercell calculations, the dipole moment might introduce systematic errors in the work function and total energy.[36] We have calculated the dipole corrections for a single OH in a 5×5 unit cell, and found that the energy change is smaller than 0.01 eV, indicating a negligible dipole correction for the systems under investigation.

III. RESULTS AND DISCUSSIONS

A. Isolated functional group on graphene

First, we consider two kinds of isolated functional groups (epoxy and hydroxyl) on graphene with supercell size varying from 2×2 to 6×6. The existence of these groups on oxidized graphene has been well established by experimental investigation.[23–25] They can be regarded as double-site and single-site impurities on the graphene plane, respectively. Hence, the study of an isolated group will be important for investigating impurity scattering and doping effects of adsorbates on graphene. As listed in Table I, the adsorption energy with respect to pure graphene and isolated atoms for each group converges to a limiting value as the supercell size increases (−4.72 eV for epoxide and −9.34 eV for hydroxyl, as obtained from calculations using a 5×5 unit cell).

TABLE I. Adsorption energy for isolated epoxy and hydroxyl units in different graphene supercells. The energy is in electron volt and with respect to free atoms.

	2×2	3×3	4×4	5×5	6×6
Epoxy	−4.68	−4.74	−4.73	−4.72	−4.73
Hydroxyl	−9.17	−9.24	−9.34	−9.34	−9.33

A single epoxy or hydroxyl functional group on graphene can induce significant local distortion. The detailed local structure for the two cases is given in Figs. 1(a) and 1(b), respectively. In Fig. 1(a), an epoxy group has one O atom bridging over two neighboring carbon atoms. The relaxed C—O bond length is 1.44 Å, larger than the C—O bond length in CO_2 (1.22 Å) but very close to that in CO (1.42 Å). It is well known that LDA errors for the bond length and bond angle are on the order of 1–2 % as compared with experimental results. The two carbon atoms connected to the O atom move upward by 0.34 Å, resulting in significant structural distortions on the graphene backbone. These two carbon atoms are separated by 1.51 Å, which is 6.3% larger than the value of 1.42 Å in the graphene plane.

Figure 1(b) shows the relaxed structure for an OH group on graphene. The O atom is on top of a carbon atom with the C—O bond nearly perpendicular to the graphene plane. The C atom bonded with the O atom moves upward by 0.37 Å relative to its three nearest-neighbor (NN) carbon atoms, enlarging the C—C bond length to 1.48 Å. This value is very close to that of the C—C bond length with sp^3-sp^2 bonding (1.50 Å).[37] The O—H bond length is 0.98 Å, slightly longer than that of the OH bond in H_2O (0.96 Å). The C—O—H bond angle is 107.9°, slightly larger than the bond angle of 104.4° in H_2O. The C—O bond length is 1.47 Å. With a new bond formed between C and O, the bonding characteristics of the connecting C atom change from planar sp^2 to distorted sp^3 hybridization for both epoxy

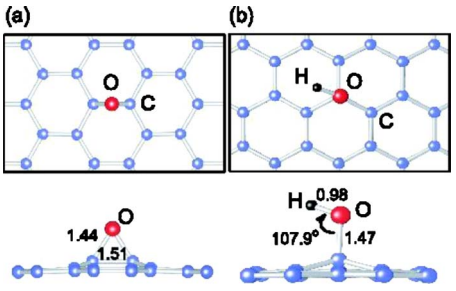

FIG. 1. (Color online) Relaxed structure for a single (a) epoxy and (b) hydroxyl group on graphene calculated using a 4×4 supercell.

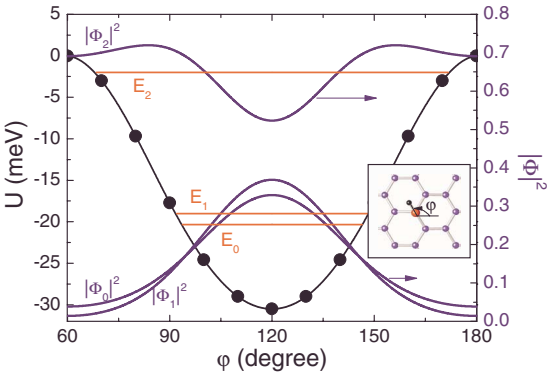

FIG. 2. (Color online) Potential $U(\varphi)$ for the OH bond rotation around the carbon atom attached to the OH group. The C—O—H angle and the distance between H and C are fixed. The three lowest eigenvalues are shown, together with their density distribution. Note that Φ_2 has been shifted by 0.5 along the y axis.

and hydroxyl groups. The structures obtained in our calculations are in good agreement with those reported in previous theoretical studies.[1,38]

Note that the orientation of the OH bond on the graphene plane points to the center of a hexagonal ring. Since the H atom (proton) is much lighter than other atoms in the system, the zero-point motion may be important. To estimate this effect, we have calculated the energy variation when the OH bond rotates around the carbon atom underneath. (Our calculations show that the bending of the OH bond will induce a much larger energy change, therefore this freedom can be safely fixed.) To the first-order approximation, one can treat only the H atom quantum mechanically. The calculated potential $U(\varphi)$ for H rotating around the C atom is shown in Fig. 2. Keeping the C—O bond length and the C—O—H bond angle fixed, the wave function $\Phi(\varphi)$ satisfies $\hat{H}\Phi(\varphi)=E\Phi(\varphi)$, with $\hat{H}=-\frac{\hbar^2 d^2}{2\mu R^2 d\varphi^2}+U(\varphi)$, where μ is the proton mass and R is the distance between H and the C—O axis. Note that the potential has a threefold symmetry: $U(\varphi+2\pi/3)=U(\varphi)$. Therefore, there are three potential wells in the 360° range. Since the energy barrier between adjacent wells is only 30 meV, there is coupling between them. The wave function can be written as $\Phi(\varphi)=e^{ik\varphi}u_k(\varphi)$, where k is an integer and could be restricted to one of the three values −1, 0, and 1, and $u_k(\varphi)$ has the same periodicity as the potential $U(\varphi)$. Solve this eigenvalue problem, one obtains three lowest levels with one singlet $E_0=9.7$ meV (for $k=0$), and one doublet $E_1=11.0$ meV (for $k=\pm 1$). For these states, the wave functions are mainly localized around $\varphi=0°$, 120°, or 240°. The next level is $E_2=28.0$ meV, only 18 meV higher, but the wave function is no longer confined in the potential well. This indicates that at room temperature, the H atom could be excited to this state.

Now we turn to the effects of the functional groups on the electronic properties of graphene. Many interesting properties have been reported for adsorbates on graphite surface[39–42] and defects on epitaxial graphene.[43] These adsorbed molecules strongly perturb the surface electronic charge density, giving rise to periodic oscillations that emanate from the defect with the same physical origin as Friedel

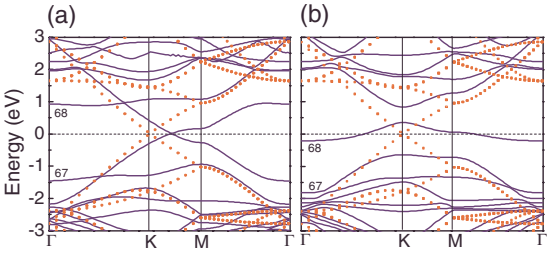

FIG. 3. (Color online) Band dispersion of graphene with a single (a) epoxy and (b) hydroxyl group calculated using a 4×4 supercell. The dotted lines show the folded band dispersions of graphene for the 4×4 supercell. Here Γ, K, and M are special points in the supercell Brillouin zone. The Fermi level has been shifted to zero. The band numbers of states near the Fermi level are indicated.

oscillations in metals. In Figs. 3(a) and 3(b), we show the band dispersions for the configurations of a single epoxy and hydroxyl group in a 4×4 graphene supercell, respectively. The folded band dispersion of graphene for the 4×4 supercell is also shown for comparison. Distinct effects of the two groups can be seen. The corresponding normalized density of states (DOSs) are shown in Figs. 4(a) and 4(b), wherein the DOS for clean graphene is also shown for comparison.

In the case of epoxide, at low concentrations (as high as one in every 2×2 unit cell) the O $2p$ orbital strongly hybridizes with the extended $\pi(\pi^*)$ bands in graphene, leading to a shift of the Dirac point in the k space and a significant reduction in the Fermi velocity ($v_F=3.7\times10^5$ m/s in a 4×4 supercell calculation). Correspondingly, the DOS near the Fermi level becomes steeper than that of the pure graphene. This change may have some important effect on the transport properties of graphene. When the concentration becomes higher (for example, a single epoxide in a 2×1 unit cell), a gap opens arising from nearly exhaustive bonding between O and carbon π states. In contrast, a single OH group has a different effect on the electronic properties of graphene, as shown in Fig. 3(b). The existence of an OH group induces a flat band at the Fermi level, leading to a small peak in the DOS. This state is half filled if a neutral OH group is included in the calculation, and will be com-

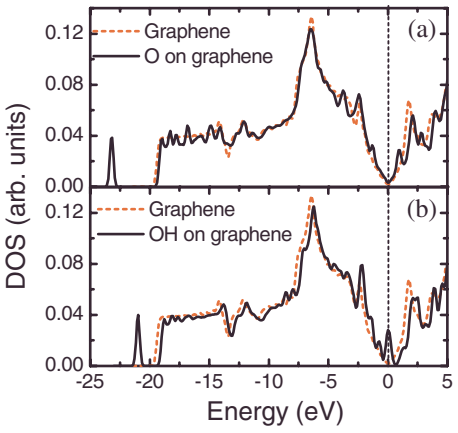

FIG. 4. (Color online) Density of states (DOS) of graphene with a single (a) epoxy and (b) hydroxyl group calculated using a 4×4 supercell. The Fermi level has been shifted to zero.

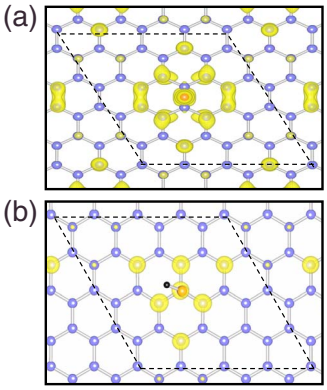

FIG. 5. (Color online) Isosurface of the charge-density distribution for the highest occupied state at Γ for graphene with a single (a) epoxy (band No.: 67) and (b) hydroxyl (band No.: 68) group calculated using a 4×4 supercell. The band numbers have been indicated in Fig. 3, respectively. The dashed lines indicate the unit cell in each case. The isovalue is 0.005 $e/\text{Å}^3$.

pletely filled if the unit is charged (i.e., hydroxyl radical, OH^{-1}). There is a small gap (about 0.14 eV, the exact value depends on the concentration of OH group) between this OH band and upper bands. The origin of this gap opening can be ascribed to two reasons: (i) breakdown of the sublattice symmetry in graphene by the OH group; and (ii) change in carbon hybridization from sp^2 to sp^3 due to strong covalent bonding between C and O.

In Figs. 4(a) and 4(b), a separate DOS peak between −20 and −25 eV can be identified. These peaks correspond mainly to the 2*s* orbital of O from the epoxy and hydroxyl groups. However, the peak location for an epoxy group is about 2 eV lower than that of a hydroxyl group. This feature might be useful for identifying existence of epoxy and hydroxyl groups in experiment.

Figures 5(a) and 5(b) show the band-decomposed charge-density distributions for the highest occupied state at the Γ point. Clearly, these functional groups induce bound states on graphene. The epoxy group induces a bound state with the C_{2v} symmetry. The hydroxyl group also induces a localized state with a threefold symmetry, which arises from the hybridization of the O $2p$ orbital with the $2p_z$ orbitals of the connected C atom and its first and the third NN carbon atoms. This localized electronic signature is very similar to the impurity state in graphene reported by Wehling *et al.*[44] and also analogous to the situation with a single carbon vacancy in graphene.[45]

B. Aggregation of functional groups on graphene

Of particular interest is the distribution of these functional groups on the graphene plane. A recent atomic force microscope measurement showed that the oxidized graphene sheets appear to have a thickness equal to integer multiples of $h\approx6.7$ Å,[46] indicating that epoxy and hydroxyl groups are most likely to be present on both sides of the graphene sheet. Hence, we will concentrate on possible two-sided configurations throughout this work.

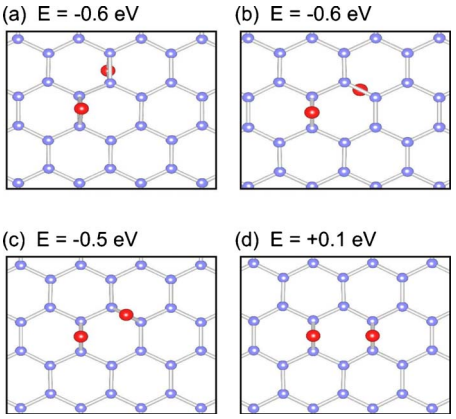

FIG. 6. (Color online) Atomic configurations for two epoxy groups on the graphene surface. The energy shown is calculated using a 5×5 unit cell and is in reference to the energy of isolated epoxy units. The O atoms are represented by larger spheres.

To find out whether these functional groups prefer to aggregate or not, we calculate the aggregation energy in reference to the energy of isolated units. Possible combinations of two epoxy (O+O, or 2O) and two hydroxyl (OH+OH, or 2OH) groups are shown in Figs. 6 and 7, respectively. The aggregation energy for the fully relaxed atomic arrangements are indicated. As can be seen from the figure, the energies are lowered considerably when these epoxy and hydroxyl units are grouped together. In particular, the most favorable configurations for two epoxy groups are those with the two units staying next to each other on opposite sides of graphene, as shown in Figs. 6(a) and 6(b), respectively. For two hydroxyl groups, significant energy gain is found for the OH units forming 1,2-hydroxyl pairs on opposite sides of the sheet [Fig. 7(a)]. This configuration is 0.3 eV lower in energy than the second favorable 1,4-paired hydroxyl groups which are on the same side of the plane. Note that the OH bond points to the O atom of the neighboring OH group [Figs. 7(b) and 7(d)], indicating a hydrogen-bond formation between the OH groups. Lahaye *et al.*[30] showed that a single OH group might

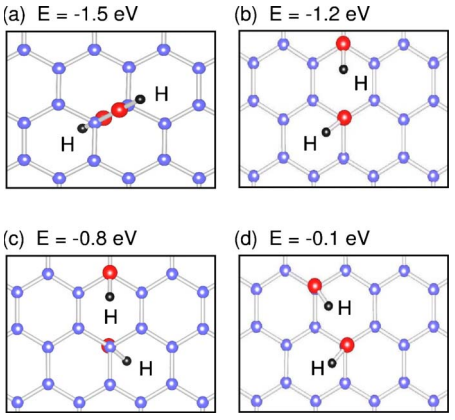

FIG. 7. (Color online) Atomic configurations for two hydroxyl groups on the graphene surface. The energy shown is calculated using a 5×5 unit cell and is in reference to the energy of isolated hydroxyl units. C and O atoms are represented by large spheres, and H by small spheres.

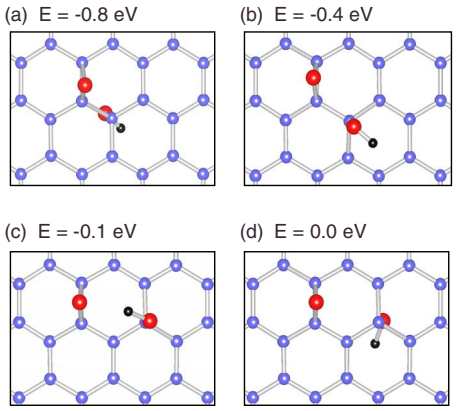

FIG. 8. (Color online) Atomic configurations for combined O +OH groups on the graphene surface. The energy shown is calculated using a 5×5 unit cell and is in reference to the energy of isolated epoxy and hydroxyl units. C and O atoms are represented by large spheres, and H by small spheres.

induce magnetic properties in oxidized graphene. However, our calculations showed that the energy gain for two OH groups to form a 1,2-hydroxyl pair is quite significant (see Fig. 7). In this case, the electrons in the system are all paired and unlikely to create a magnetic system.

The relaxed atomic structures for combinations of both epoxy and hydroxyl groups are shown in Figs. 8–11. These combinations include: (i) O+OH, (ii) O+2OH, (iii) 2O +OH, and (iv) 2O+2OH. For each case, we show multiple configurations together with their aggregation energy gains. Clearly, these functional groups prefer to form aggregates. One of the reasons is the cancellation of vertical structural distortion when these units can be located on both sides of the sheet. From Figs. 6–11, we conclude that: (i) the OH units form 1,2-hydroxyl pairs [Fig. 7(a)] on opposite sides of the sheet; and (ii) the combination of O+2OH and 2O +2OH are particularly favorable [Figs. 9(a) and 11(a)]. In Figs. 9(a), 10(a), and 11(a), H points toward the neighboring O on the same side, yielding a configuration characterized by a hydrogen bond. The results in Figs. 6–11 indicate that these

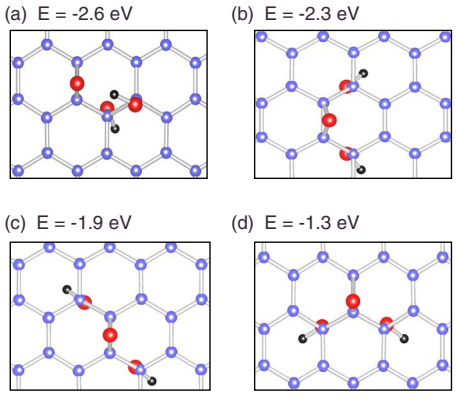

FIG. 9. (Color online) Atomic configurations for combined O +2OH groups on the graphene surface. The energy shown is calculated using a 5×5 unit cell and is in reference to the energy of isolated epoxy and hydroxyl units. C and O atoms are represented by large spheres, and H by small spheres.

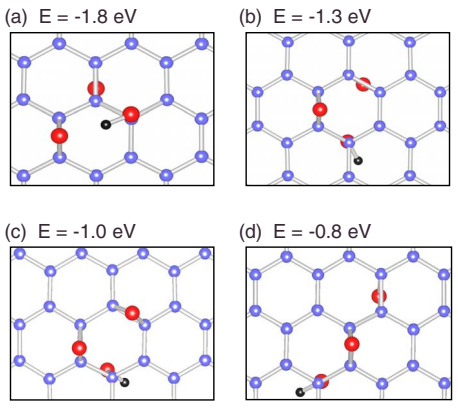

FIG. 10. (Color online) Atomic configurations for combined 2O+OH groups on the graphene surface. The energy shown is calculated using a 5×5 unit cell and is in reference to the energy of isolated epoxy and hydroxyl units. C and O atoms are represented by large spheres, and H by small spheres.

adsorbed units prefer to stay close to each other on the graphene surface. This is in full agreement with the experimental results inferred from the NMR data.[23–25]

In Fig. 12, we show the DOSs for representative combinations of the functional groups. In the case of O+OH [Fig. 12(a)], there is a clear peak at the Fermi level. This state is induced by the neutral OH group with an odd number of electrons in the supercell. There are two well-separated O 2*s* peaks (at around −23 eV and −21 eV) far below the Fermi level corresponding to the epoxy and OH groups, respectively. This feature is consistent with that in the DOS for isolated single groups. In Figs. 12(b) and 12(c), the 1,2-hydroxyl pairs remove the localized state at the Fermi level, opening a small band gap (around 0.1 eV) in the system. Interestingly, in the case of O+2OH [Fig. 12(c)], there are three O 2*s* peaks corresponding to the epoxy and two OH groups, respectively. This indicates that the O 2*s* peak positions are distinguishable for the epoxy and hydroxyl groups.

Vibrational modes can be used as a characteristic signature for the functional groups. We have calculated the local-

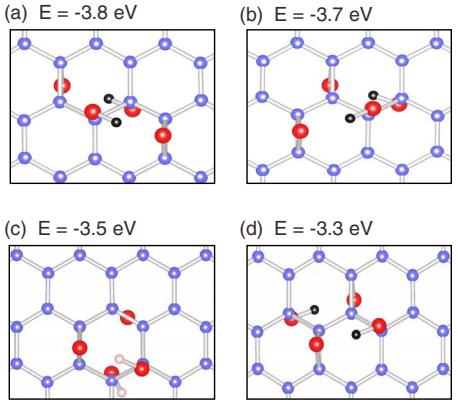

FIG. 11. (Color online) Atomic configurations for combined 2O+2OH on the graphene surface. The energy shown is calculated using a 5×5 unit cell and is in reference to the energy of isolated epoxy and hydroxyl units. C and O atoms are represented by large spheres, and H by small spheres.

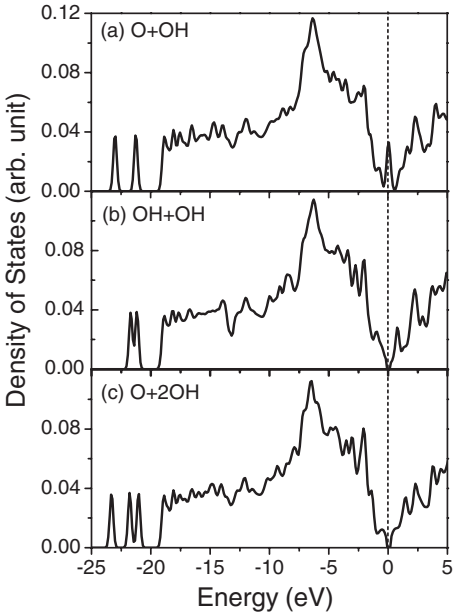

FIG. 12. Densities of states for the combinations of epoxy and hydroxyl groups on graphene calculated using a 4×4 supercell: (a) O+OH, (b) OH+OH, and (c) O+2OH.

ized vibrational properties of the 1,2-hydroxyl pair in a 4 $\times$4 unit cell using the QUANTUM-ESPRESSO code.[47] Norm-conserving pseudopotentials for C, H, and O have been employed. The optimized structures have been reevaluated using the QUANTUM-ESPRESSO code and the optimal structures are found to be very similar to those obtained from VASP calculations. The two stretching modes induced by the OH groups are shown in Figs. 13(a) and 13(b), respectively. The frequencies of the two modes are around 3656 cm^{-1}. In contrast, the calculated frequency for the C—H stretching mode of a single H absorbed on graphene in a 4×4 unit cell is found to be about 2600 cm^{-1}. These vibrational modes might be useful to identify the functional groups on graphene.[48,49]

C. Possible ordered structures for graphene oxide

In this section, we explore possible ordered phases containing epoxy and hydroxyl groups incorporating the energetically favorable building blocks found in the previous section. Based on these energetics results, only the epoxy group and 1,2-hydroxyl pairs on graphene will be included in the current study.

A variety of possible structures with only oxygen on the graphene surface have been studied.[29,31,50] The configurations with epoxy pairs on the same two carbon atoms have been considered in a recent theoretical calculation.[31] It was found that an isolated epoxy pair is less stable than a carbonyl pair; this provided an atomic mechanism to "unzip" the graphene sheet.[31] If one finds a way to keep these epoxy pairs, a new low-energy phase consisting of chains of these epoxy pairs was proposed.[50] In a recent work by Xu *et al.*,[29] graphene epoxide covered with asymmetric unzipped epoxy groups is shown to be more stable than normal epoxy groups.

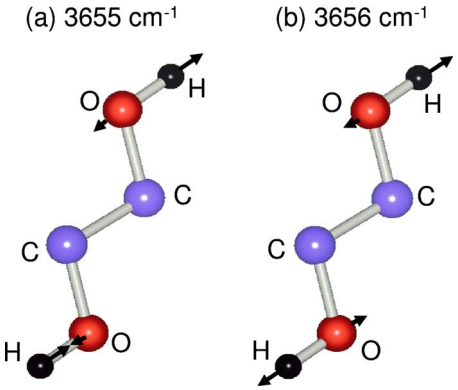

FIG. 13. (Color online) O—H stretching modes for 1,2-hydroxyl pairs shown in Fig. 7(a) calculated using a 4×4 unit cell.

However, the line up of unzipped epoxide is believed to be the formation mechanism for fault lines observed in oxidized graphene and graphite.[31] In the current study, we focus on the interplay of epoxy and hydroxyl units on the graphene surface before the graphene sheet disintegrates. Following the conclusion from the most recent NMR data,[25] we limit our study to configurations with normal epoxy groups only. Figures 14(a) and 14(b) show the relaxed atomic structures for two different configurations with unit cells C_4O_2 and C_6O_3, respectively.

The energy of the configuration in Fig. 14(a) is 0.3 eV per C_2O lower than that of the configuration in Fig. 14(b). In Fig. 14(a), the epoxy groups follow Fig. 6(a) and stay in rows on opposite sides of the sheet. The line up of epoxy groups on both sides of graphene compensates the structural buckling and exhibits a rectangular unit cell of 2.55 Å $\times$4.40 Å. This is comparable to a recent UHV scanning tunnel microscope study[46] where a local periodicity with a unit cell of 2.73 Å$\times$4.06 Å was reported in some region of graphene oxide. Despite of a discrepancy of 8–9 % in individual lattice parameters, we note that the area of our calculated unit cell is within 1.2% of the experimental value. Other causes, for example, the substrate effect, might influence the measured lattice parameters. Similar results for

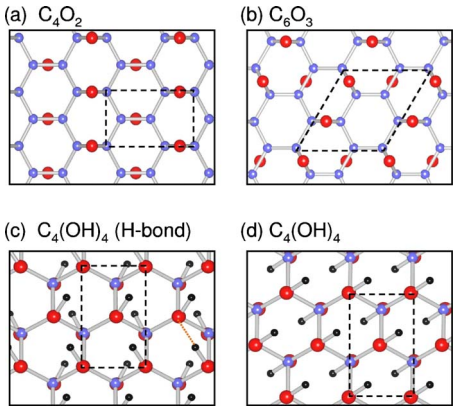

FIG. 14. (Color online) Calculated structures for the fully oxidized ideal phases covered by only epoxy or hydroxyl groups. (a) C_4O_2, (b)C_6O_3, (c) $C_4(OH)_4$ with H bonds, and (d) $C_4(OH)_4$ without H bond.

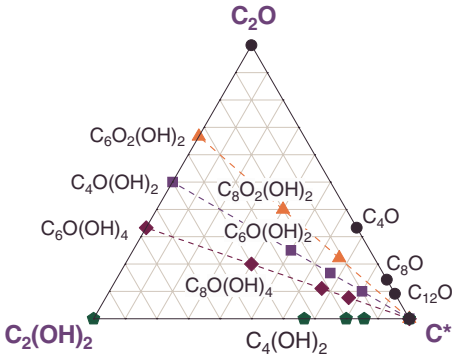

FIG. 15. (Color online) Ternary diagram showing ordered phases on the graphene surface with different amounts of sp^2 Carbon (C^*), epoxide (C_2O), and the 1,2-hydroxyl pair ($C_2(OH)_2$). The phases investigated in this study are marked on the diagram, with dashed lines indicating those with the same relative amount of epoxide and hydroxyl pairs.

epoxy-only structures were also reported by other groups.[1,28,29]

For graphene fully covered with hydroxyl groups, two energetically favorable atomic structures with formula $C_4(OH)_4$ are shown in Figs. 14(c) and 14(d). Although the theoretical composition of $C_4(OH)_4$ has not been observed in experiment, the calculated structures will be useful to illustrate the key features of intermediate phases below. In Fig. 14(c), one can easily identify that the 1,2-hydroxyl pairs are connected to form a chainlike structure on both sides of the sheet in such a way that the interaction associated with hydrogen bonds can be maximized. The formation of hydrogen bonds between OH groups lowers the energy by 0.2 eV per unit cell as compared to the configuration shown in Fig. 14(d).

We now study the intermediate coverage with various relative coverages of epoxy and OH groups. Previous work by Boukhvalov and Katsnelson[28] employed the energies of H_2O and O_2 molecules as the reference points for calculating the chemical potentials for the O and OH groups. Here we are concerned with the relative stability of phases with different coverages and will adopt an approach frequently used for a ternary system by investigating the relative formation energy. Based on the energetics results, we consider only arrangements with the OH group appearing in 1,2-hydroxyl pairs, as shown in Fig. 7(a). Each periodic phase can be specified by the relative amount of "free" sp^2 C atoms (denoted by C^*, corresponding to C atoms not bonded to O), epoxide (C_2O) as shown in Fig. 1(a), and the 1,2-hydroxyl pair [$C_2(OH)_2$ with the connecting C atoms included]. To compare the stability for different coverages, one needs to find a way to define the formation energy for this three-component system. The representative stoichiometry is $C^*_{1-x-y}(C_2O)_x[C_2(OH)_2]_y$, or equivalently $C_{1+x+y}O_x(OH)_{2y}$, with $0 \le x \le 1$, $0 \le y \le 1$, and $0 \le x+y \le 1$. The ordered phases we have calculated are marked on a ternary diagram shown in Fig. 15, where the dashed lines indicate phases with the same ratio of the epoxy group versus the hydroxyl pair. For each phase we investigated, the structure was optimized by exploring various different local arrangements of the epoxy and hydroxyl groups. The lattice parameters and atomic coordinates are fully relaxed. The formation energy is defined in the usual way for a ternary system,

$$\Delta E[x,y] = E[C_{1+x+y}O_x(OH)_{2y}] - (1-x-y)E[C^*] - xE[C_2O] - yE[C_2(OH)_2], \quad (1)$$

where $E[Z]$ represents the energy of a periodic phase Z. The detailed formation energies have been presented in our previous publication.[32] For completeness, we listed these results in Table II, together with the calculated cohesive energy for each phase. Below we report more detailed structural and electronic properties marked in Fig. 15.

TABLE II. Calculated cohesive energies (E_{coh}) and formation energies (E_f) for the fully oxidized and intermediate phases.

	E_{coh} (eV/f.u.)	E_f (eV)
C_4O_2	−51.961	0.000
$C_6O_2(OH)_2$	−94.902	−0.157
$C_{16}O_4(OH)_8$	−275.025	−0.153
$C_6O(OH)_4$	−111.268	−0.115
$C_4(OH)_4$	−84.941	0.000
C_4O_2	−51.961	0.000
C_4O	−46.169	0.026
C_8O	−86.722	0.008
$C_{12}O$	−127.252	0.006
C	−10.133	0.000
$C_{12}O_4(OH)_4$	−189.803	−0.157
$C_{16}O_4(OH)_4$	−229.209	0.019
$C_{24}O_4(OH)_4$	−310.409	0.003
$C_{16}O_4(OH)_8$	−275.025	−0.153
$C_{12}O_2(OH)_4$	−176.854	0.073
$C_{16}O_2(OH)_4$	−217.553	0.035
$C_{24}O_2(OH)_4$	−298.558	0.024
$C_{24}O_4(OH)_{16}$	−445.071	−0.115
$C_{16}O_2(OH)_8$	−262.108	0.027
$C_{24}O_2(OH)_8$	−343.310	0.007
$C_32O_2(OH)_8$	−424.304	0.008
$C_4(OH)_4$	−84.941	0.000
$C_8(OH)_4$	−124.969	0.084
$C_{12}(OH)_4$	−165.367	0.064
$C_{16}(OH)_4$	−205.864	0.048

The formation energy for the fully oxidized phases with mixed epoxide and hydroxyl compositions is negative,[32] indicating that these intermediate phases are stable against separation into pure epoxide and pure hydroxyl phases. These stable phases include $C_{12}O_4(OH)_4$, $C_{16}O_4(OH)_8$, and $C_{24}O_4(OH)_{16}$, with an epoxide to hydroxyl ratio of 1:1, 1:2, and 1:4, respectively. The structures are shown in Figs. 16(a), 16(c), and 16(e). The arrangement of hydroxyl groups follows the same pattern as shown in Fig. 14(c): the 1,2-hydroxyl pairs are connected to form a chainlike structure on both sides of the sheet. In addition, O atoms are drawn to the

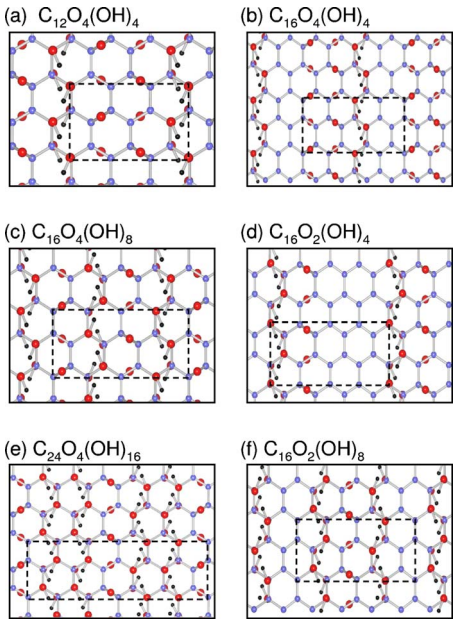

FIG. 16. (Color online) Calculated low-energy structures for representative ordered phases covered by both epoxy and hydroxyl groups. The dashed lines indicate the unit cell in each case.

remaining C atoms in the same hexagonal rings to form epoxides in close proximity. This is consistent with the energy analysis in the previous section that epoxy and hydroxyl groups tend to aggregate in the same hexagonal ring, as shown in Figs. 11(a) and 11(b). These features turn out to be quite energetically favorable in constructing phases with intermediate compositions. Boukhvalov *et al.* (Ref. 28) concluded that $C_8O(OH)_4$ is the "most stable" configuration of graphene functionalized by both oxygen and hydroxyl groups. We find that the structure given in Figs. 1c and 4e of Ref. 28 turns out to be 0.4 eV (per eight C atoms) higher in energy than our optimized structure using a unit cell twice large.

A brief comment on the hydrogen bond might be instructive. It is well known that hydrogen bond exists commonly in biological macromolecules and liquid systems such as water. In crystals, the hydrogen bond is relatively weaker than other bonding types, such as covalent, ionic, and metallic bonds. However, as the concentration of OH groups becomes higher, the H atom will be attracted by the O atom of the OH group at the nearest-neighbor site. In this case, the long chainlike structures could form, resulting in a significant decrease in the total energy. Typically, the hydrogen bond has an energy in the range of 5–30 kJ/Mol. In water, the hydrogen-bond energy is about 21 kJ/mol, i.e., 0.2 eV/bond. In graphene oxide, the energy associated with the OH$\cdots$O configuration is estimated to be about 0.05 eV/bond. Hence, the orientations of the OH groups will play a significant role in minimizing the system's energy. As a consequence, hydroxyl groups on the graphene surface tend to interact and form chainlike structures stabilized by hydrogen bonding.

Apart from the fully oxidized graphene with both epoxy and hydroxyl groups, we could not find other ordered phases with a negative formation energy in our calculations. Therefore, we infer that the $T=0$ lowest-energy configuration of the graphene oxide sheet is likely to be a combination of fully oxidized regions and the clean graphene phase. However, since the oxidation process is a highly nonequilibrium one, domains of various intermediate phases may still be found in the sample under experimental conditions. The relative amount of epoxy and hydroxyl units on the graphene sheet depends on the sample preparation process and can vary over a wide range. Below we focus on phases along each dashed line in Fig. 15, in which the relative amount of epoxy and hydroxyl units on the surface is a constant.

After exploring various configurations, we find that the lowest-energy periodic structure of these intermediate phases contains strips of epoxide and hydroxyl combinations with clean graphene ribbons in between. For example, the structures of $C_{16}O_4(OH)_4$, $C_{16}O_2(OH)_4$, and $C_{16}O_2(OH)_8$ are shown in Figs. 16(b), 16(d), and 16(f), respectively, which contain separate regions of sp^2 and sp^3 carbon. The sp^3 strips consist of hydroxyl chains on both sides of the plane and neighboring epoxides. The strips interact weakly when separated by carbon ribbons with sp^2 C^* composition larger than about 0.4. (Phases with different C^* compositions have different strip separations.) With the formation energies falling on a near straight line as shown in Fig. 2(b) in Ref. 32, many of these phases are expected to coexist on the surface. It is energetically favorable for these strips to coalesce since the fully oxidized phase has a lower formation energy. However, this process may not be completed during the sample preparation.

Based on the results discussed above, we arrive at the following conclusion for the distribution of epoxy and hydroxyl groups on graphene: the hydroxyl groups form chains resulting from hydrogen-bond interaction between 1,2-hydroxyl pairs which greatly lower the energy; and the epoxides are grouped next to these hydroxyl chains. Therefore, the epoxide and hydroxyl units randomly deposited on the surfaces are expected to arrange themselves locally following these patterns, giving rise to patches of sp^2 carbon surrounded by fully oxidized epoxide+hydroxyl regions or vice versa. The possible existence of pure graphene ribbons was proposed previously[26] in order to explain the shift of the Raman peaks in GO and few-layer graphenes. The current study further supports this picture based on extensive first-principles calculations.

The finite region of sp^2 carbon has an interesting consequence in the electronic structure of graphene oxide. Without knowing the exact atomic arrangements at various compositions, we use the results of the ordered structures investigated above to provide an estimate for this effect. In Figs. 17 and 18, we show the calculated DOSs for the ordered phases of oxidized graphene. In the case of completely oxidized graphene, an energy gap ranging from 2.0 to 4.0 eV can be identified in Fig. 17. A considerable variation in the gap value is observed for phases with different ratios of the OH and epoxy groups, indicating that the gap opening by oxidation is dependent on the relative amount of the OH and epoxy groups. In particular, the gap size is dictated by the width of the graphene ribbons in the intermediated ordered phases we have studied. A few vanishing band gap values are associated with armchair ribbons with $3n+2$ rows of atoms (n is an integer) or zigzag ribbons with an even number of

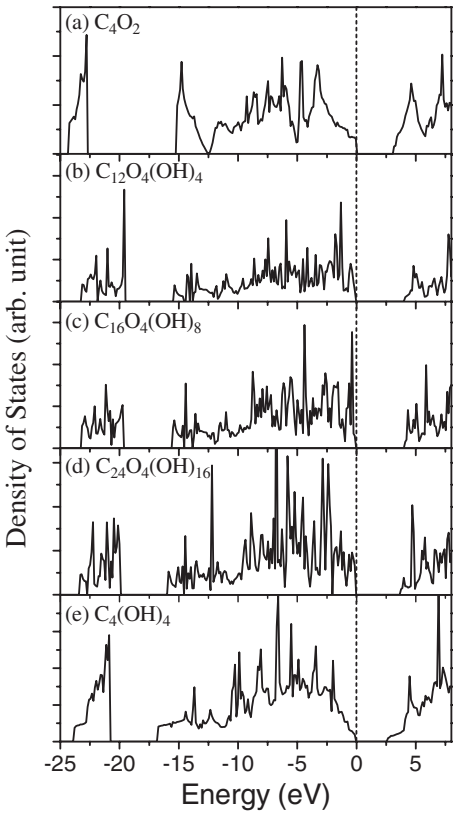

FIG. 17. Density of states for completely oxidized phases shown in Figs. 14 and 16. (a) C_4O_2, (b) $C_{12}O_4(OH)_4$, (c) $C_{16}O_4(OH)_8$, (d) $C_{24}O_4(OH)_{16}$, and (e) $C_4(OH)_4$. The zero energy is set at the last occupied state.

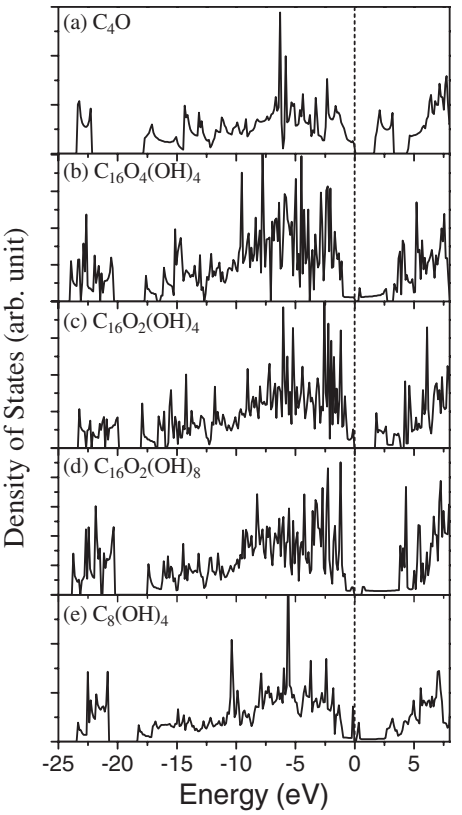

FIG. 18. Density of states for ordered phases with intermediate compositions as marked in Fig. 15. (a) C_4O, (b) $C_{16}O_4(OH)_4$, (c) $C_{16}O_2(OH)_4$, (d) $C_{16}O_2(OH)_8$, and (e) $C_8(OH)_4$. The zero energy is set at the last occupied state.

atomic rows. These may be considered as special cases.

IV. SUMMARY

In summary, we have performed first-principles calculations to study the structures of the oxidation functional groups (epoxy and hydroxyl) on single-layer graphene, and the induced changes in the electronic properties. Our calculations show that it is energetically favorable for the hydroxyl and epoxide groups to aggregate together and to form specific types of strips with sp^2 carbon regions in between. The isolated oxidation functional groups can induce interesting bound states, which might have important effects on the transport properties of graphene after reduction treatment. By changing the oxidation level and the relative compositions of the epoxy and hydroxyl groups, significant band gaps can be developed in graphene oxide, suggesting a great potential to tune the energy gap in graphene through controlled oxidation processes.

It is interesting to note that hydrogen bonding appears to play a significant role in determining the structure of these oxidized phases, yielding chainlike structures for the OH groups. Although the probability of forming a large-domain chainlike structures could be strongly dependent on the oxidation process, the local aggregation of OH and epoxy groups may follow the ordered phases discussed in this work.

ACKNOWLEDGMENTS

We thank P. N. First and W. Y. Ruan for discussions and S. Barraza-Lopez for the assistance with some plots. This work is supported by the Department of Energy (Grant No. DE-FG02-97ER45632). We acknowledge interaction with the Georgia Tech MRSEC funded by National Science Foundation (Grant No. DMR-08-20382). This research used computational resources at the National Energy Research Scientific Computing Center, which is supported by the Office of Science of the U.S. Department of Energy under Contract No. DE-AC02-05CH11231, and the National Science Foundation TeraGrid resources provided by the Texas Advanced Computing Center (TACC).

[1] J.-L. Li, K. N. Kudin, M. J. McAllister, R. K. Prud'homme, I. A. Aksay, and R. Car, Phys. Rev. Lett. **96**, 176101 (2006).
[2] D. A. Dikin, S. Stankovich, E. J. Zimney, R. D. Piner, G. H. B. Dommett, G. Evmenenko, S. T. Nguyen, and R. S. Ruoff, Nature (London) **448**, 457 (2007).
[3] G. Eda, G. Fanchini, and M. Chhowalla, Nat. Nanotechnol. **3**, 270 (2008).
[4] T. Echtermeyer, M. Lemme, M. Baus, B. Szafranek, A. Geim, and H. Kurz, arXiv:0712.2026 (unpublished).
[5] X. Wu, M. Sprinkle, X. Li, F. Ming, C. Berger, and W. A. de Heer, Phys. Rev. Lett. **101**, 026801 (2008).
[6] D. W. Boukhvalov, M. I. Katsnelson, and A. I. Lichtenstein, Phys. Rev. B **77**, 035427 (2008).
[7] D. C. Elias, R. R. Nair, T. M. G. Mohiuddin, S. V. Morozov, P. Blake, M. P. Halsall, A. C. Ferrari, D. W. Boukhvalov, M. I. Katsnelson, A. K. Geim, and K. S. Novoselov, Science **323**, 610 (2009).
[8] I. Jung, D. A. Dikin, R. D. Piner, and R. S. Ruoff, Nano Lett. **8**, 4283 (2008).
[9] G. Eda, C. Mattevi, H. Yamaguchi, H. Kim, and M. Chhowalla, J. Phys. Chem. C **113**, 15768 (2009).
[10] Z. Luo, P. M. Vora, E. J. Mele, A. T. Charlie Johnson, and J. M. Kikkawaa, Appl. Phys. Lett. **94**, 111909 (2009).
[11] D. Li, M. B. Muller, S. Gilje, R. B. Kaner, and G. G. Wallace, Nat. Nanotechnol. **3**, 101 (2008).
[12] H. C. Schniepp, J. L. Li, M. J. McAllister, H. Sai, M. Herrera-Alonso, D. H. Adamson, R. K. Prud'homme, R. Car, D. A. Saville, and I. A. Aksay, J. Phys. Chem. B **110**, 8535 (2006).
[13] C. Gómez-Navarro, R. T. Weitz, A. M. Bittner, M. Scolari, A. Mews, M. Burghard, and K. Kern, Nano Lett. **7**, 3499 (2007).
[14] S. Gilje, S. Han, W. Minsheng, L. W. Kang, and R. B. Kaner, Nano Lett. **7**, 3394 (2007).
[15] S. Stankovich, D. A. Dikin, R. D. Piner, K. A. Kohlhaas, A. Kleinhammes, Y. Jia, Y. Wu, S. T. Nguyen, and R. S. Ruoff, Carbon **45**, 1558 (2007).
[16] Z. Luo, Y. Lu, L. A. Somers, and A. T. Charlie Johnson, J. Am. Chem. Soc. **131**, 898 (2009).
[17] T. Nakajima, A. Mabuchi, and R. Hagiwara, Carbon **26**, 357 (1988).
[18] A. Buchsteiner, A. Lerf, and J. Pieper, J. Phys. Chem. B **110**, 22328 (2006).
[19] G. L. Ruess, Kolloid Z. **110**, 17 (1945).
[20] A. Clause, R. Plass, H.-P. Boehm, and U. Hofmann, Z. Anorg. Allg. Chem. **291**, 205 (1957).
[21] M. Mermoux, Y. Chabre, and A. Rousseau, Carbon **29**, 469 (1991).
[22] T. Nakajima and Y. Matsuo, Carbon **32**, 469 (1994).
[23] A. Lerf, H. He, M. Forster, and J. Klinowski, J. Phys. Chem. B **102**, 4477 (1998).
[24] H. He, J. Klinowski, M. Forster, and A. Lerf, Chem. Phys. Lett. **287**, 53 (1998).
[25] W. Cai, R. D. Piner, F. J. Stadermann, S. Park, M. A. Shaibat, Y. Ishii, D. Yang, A. Velamakanni, S. J. An, M. Stoller, J. An, D. Chen, and R. S. Ruoff, Science **321**, 1815 (2008).
[26] K. N. Kudin, B. Ozbas, H. C. Schniepp, R. K. Prud'homme, I. A. Aksay, and R. Car, Nano Lett. **8**, 36 (2008).
[27] J. T. Paci, T. Belytschko, and G. C. Schatz, J. Phys. Chem. C **111**, 18099 (2007).
[28] D. W. Boukhvalov and M. I. Katsnelson, J. Am. Chem. Soc. **130**, 10697 (2008).
[29] Z. Xu and K. Xue, Nanotechnology **21**, 045704 (2010).
[30] R. J. W. E. Lahaye, H. K. Jeong, C. Y. Park, and Y. H. Lee, Phys. Rev. B **79**, 125435 (2009).
[31] Z. Li, W. Zhang, Y. Luo, J. Yang, and J. G. Hou, J. Am. Chem. Soc. **131**, 6320 (2009).
[32] J. A. Yan, L. Xian, and M. Y. Chou, Phys. Rev. Lett. **103**, 086802 (2009).
[33] G. Kresse and J. Hafner, Phys. Rev. B **47**, 558 (1993).
[34] D. Vanderbilt, Phys. Rev. B **41**, 7892 (1990).
[35] H. J. Monkhorst and J. D. Pack, Phys. Rev. B **13**, 5188 (1976).
[36] L. Bengtsson, Phys. Rev. B **59**, 12301 (1999).
[37] F. A. Carey and R. J. Sundberg, *Advanced Organic Chemistry*, 3rd ed. (Plenum Press, New York, 1990).
[38] K. A. Mkhoyan, A. W. Contryman, J. Silcox, D. A. Stewart, G. Eda, C. Mattevi, S. Miller, and M. Chhowalla, Nano Lett. **9**, 1058 (2009).
[39] H. A. Mizes and J. S. Foster, Science **244**, 559 (1989).
[40] K. F. Kelly, E. T. Mickelson, R. H. Hauge, J. L. Margrave, and N. J. Halas, Proc. Natl. Acad. Sci. U.S.A. **97**, 10318 (2000).
[41] P. Ruffieux, O. Gröning, P. Schwaller, L. Schlapbach, and P. Gröning, Phys. Rev. Lett. **84**, 4910 (2000).
[42] P. Ruffieux, M. Melle-Franco, O. Gröning, M. Bielmann, F. Zerbetto, and P. Gröning, Phys. Rev. B **71**, 153403 (2005).
[43] G. M. Rutter, J. N. Crain, N. P. Guisinger, T. Li, P. N. First, and J. A. Stroscio, Science **317**, 219 (2007).
[44] T. O. Wehling, A. V. Balatsky, M. I. Katsnelson, A. I. Lichtenstein, K. Scharnberg, and R. Wiesendanger, Phys. Rev. B **75**, 125425 (2007).
[45] G. Trambly and D. Mayou (private communication).
[46] D. Pandey, R. Reifenberger, and R. Piner, Surf. Sci. **602**, 1607 (2008).
[47] S. Baroni, S. de Gironcoli, A. Dal Corso, and P. Giannozzi, Rev. Mod. Phys. **73**, 515 (2001).
[48] N. P. Guisinger, G. M. Rutter, J. N. Crain, P. N. First, and J. A. Stroscio, Nano Lett. **9**, 1462 (2009).
[49] J. O. Sofo, A. S. Chaudhari, and G. D. Barber, Phys. Rev. B **75**, 153401 (2007).
[50] H. Xiang, S. Wei, and X. Gong, Phys. Rev. B **82**, 035416 (2010).